



[^{99m}Tc]duramycin for cell death imaging: Impact of kit formulation, purification and species difference

Luca Palmieri ^{a,b,1}, Filipe Elvas ^{a,b,1}, Christel Vangestel ^{a,b}, Koon Pak ^c, Brian Gray ^c, Sigrid Stroobants ^{a,b}, Steven Staelens ^a, Leonie wyffels ^{a,b,*}

^a Molecular Imaging Center Antwerp, University of Antwerp, Campus Drie Eiken, Universiteitsplein 1, B-2610 Wilrijk, Belgium

^b Antwerp University Hospital, Department of Nuclear Medicine, Wilrijkstraat 10, B-2650, Edegem, Belgium

^c Molecular Targeting Technologies, Inc., West Chester, PA, USA

ARTICLE INFO

Article history:

Received 2 March 2017

Received in revised form 25 August 2017

Accepted 28 August 2017

Keywords:

Kit formulation

[^{99m}Tc]duramycin

Treatment response

Cell death

SPECT

ABSTRACT

Introduction: [^{99m}Tc]duramycin is a SPECT tracer for cell death imaging. We evaluated the impact of kit formulation, purification and species difference on the pharmacokinetic profile and cell death targeting properties of [^{99m}Tc]duramycin in order to define the optimal conditions for (pre-)clinical use.

Methods: Three kits were prepared (A: traditional formulation, B: containing 1/3 of ingredients, C: containing HYNIC-PEG₁₂-duramycin). Following labeling, the kits were used without purification, or with SPE or HPLC purification. The pharmacokinetic profile was evaluated in mice and rats at 24 h post tracer injection (p.i.). Non-specific accumulation of [^{99m}Tc]duramycin was studied by μ SPECT imaging in chemotherapy treated COLO205 tumor bearing mice pre-treated with cold duramycin (0.01–50 μ g). Cell death targeting ability of the kits displaying the best pharmacokinetic profile was compared in a treatment response study in COLO205 tumor bearing mice treated with conatumumab (anti-DR5 antibody).

Results: HPLC purification of kit prepared [^{99m}Tc]duramycin and reducing the amount of kit ingredients resulted in the best pharmacokinetic profile with low accumulation in liver, spleen and kidneys. The use of PEGylated [^{99m}Tc]duramycin required longer circulation times (> 4 h pi) to obtain good imaging characteristics. Pre-treatment with duramycin significantly decreased tracer uptake in chemotherapy treated tumors in a dose-dependent manner. A blocking dose of 50 μ g significantly increased non-specific accumulation in liver and spleen. Non-specific accumulation of [^{99m}Tc]duramycin was however demonstrated to be species dependent. HPLC purified kit A (5.21 ± 1.71 %ID/cc) and non-purified kit B (1.68 ± 0.46 %ID/cc) demonstrated a significant increase in tumor uptake compared to baseline following conatumumab treatment.

Conclusions: To obtain [^{99m}Tc]duramycin with favorable imaging characteristics for cell death imaging in mice [^{99m}Tc]duramycin needs to be prepared with high specific activity by applying HPLC purification. The need for HPLC purification appears to be a species dependent phenomenon and might therefore not be required for clinical translation.

© 2017 Elsevier Inc. All rights reserved.

1. Introduction

In recent years, early monitoring of tumor response to therapy has gained increasing importance in oncology to tailor individual therapies and rapidly evaluate novel cancer therapies. Currently, the most commonly used methodology to evaluate the efficiency of a therapeutic regimen is based upon the evaluation of morphological and volumetric changes in solid tumors using anatomical imaging techniques like

computed tomography (CT) and magnetic resonance imaging (MRI) and applying the Response Evaluation Criteria in Solid Tumors (RECIST) guidelines [1]. However, a major drawback of these anatomical imaging methods is that they are not sensitive enough to assess the early effectiveness of a therapy as it may take several weeks until tumor-shrinkage becomes apparent. As changes at the molecular level precede morphological changes in the tumor, molecular imaging techniques such as positron emission tomography (PET) and single photon emission computed tomography (SPECT) offer a more sensitive and specific tool for early treatment response evaluation.

It has been demonstrated that cell death plays an important role not only in the pathogenesis of cancer [2] but also in disease treatment and response evaluation. As a number of anti-cancer treatments work by the induction of apoptosis and/or necrosis in tumor cells [3,4], molecular

* Corresponding author at: Antwerp University Hospital, Department of Nuclear Medicine, Wilrijkstraat 10, B-2650, Edegem, Belgium. Tel.: +32 3 821 5699; fax: +32 3 825 3308.

E-mail address: leonie.wyffels@uza.be (L. wyffels).

¹ These authors contributed equally to this work.

imaging of cell death could represent a useful tool for early treatment response evaluation in the clinic.

Until now, a variety of cell-death imaging agents have been evaluated, both for PET and SPECT, targeting cell death markers such as externalized plasma membrane phospholipids [5–8], intracellular activation of caspase-3 [9–11], or the apoptotic cell membrane imprint [12]. The most widely investigated radiotracers for cell death imaging are based upon the 36 kDa protein annexin V which binds to externalized phosphatidylserine (PS). ^{99m}Tc -labelled annexin V-128 is currently under clinical investigation and may provide valuable information on PS exposure in different indications [13], yet annexin V based radiotracers suffer from an inherent drawback. The protein's high molecular weight results in suboptimal biodistribution and pharmacokinetics and thus low target to background ratios in imaging. In this context, there currently is a need for novel, more selective and smaller cell-death imaging agents.

Next to PS, phosphatidylethanolamine (PE) is massively expressed during the cell death process and therefore represents an excellent target for cell death imaging [14]. Duramycin is a small polypeptide (~2 kDa) which forms a stereospecific binding pocket over the ethanolamine head group [15,16], and therefore binds PE with high affinity ($K_d \sim 5$ nM) and specificity [17]. It has been labeled with ^{99m}Tc by modification of duramycin with a hydrazinonicotinamide (HYNIC) chelator for SPECT imaging of cell death [18]. The advantage of using ^{99m}Tc as a radioisotope is that it has a workable half-life of 6 h, favorable gamma photon energy characteristics, and more importantly, it is easily available making it the most widely used radionuclide for molecular imaging at this moment. Duramycin's low molecular weight confers it a favorable biodistribution and pharmacokinetic (PK) properties, promoting an efficient blood clearance and high target-to-background ratios [18]. ^{99m}Tc duramycin has been used as a probe for imaging of apoptosis in animal models of myocardial [19,20] and cerebral [21] ischemia-reperfusion, for imaging of tissue damage after whole-body irradiation [22], and hyperoxia-induced pulmonary endothelial cell-death [23], for imaging of treatment response in colorectal [24,25] and breast [26] cancer models, and for imaging of atherosclerotic plaques [27]. Zhao et al. developed a stable single-step kit for easy production of ^{99m}Tc duramycin [19]. By using a ternary ligand system for radiolabeling, comprised of HYNIC-duramycin and tricine and trisodium triphenylphosphine-3,3',3''-trisulfonate (TPPTS) as co-ligands, ^{99m}Tc duramycin could be obtained with a radiochemical purity (RCP) of >90%. Moreover, the biodistribution profile in rats of this kit-prepared ^{99m}Tc duramycin was consistent with HPLC purified ^{99m}Tc duramycin [21]. In our hands however, the use of the same kit formulation in our studies did not always result in satisfactory RCP, with low amounts of polar impurities visible in the radiochromatogram [26]. Furthermore, imaging studies in mice revealed a high non-specific accumulation of radioactivity in the liver, spleen and kidneys compared to HPLC purified ^{99m}Tc duramycin. The less optimal dosimetry and imaging properties of the kit-prepared ^{99m}Tc duramycin forced us to use the time consuming and less practical HPLC purification for imaging studies in mice. In the current study we therefore explored the impact of ^{99m}Tc duramycin kit formulation and post-labeling purification method on the RCP and biodistribution profile in mice and rats. A blocking study was performed in COLO205 tumor bearing mice treated with chemotherapy to further investigate non-specific accumulation of the radiotracer. The kits with the best imaging characteristics were evaluated in a treatment response study COLO205 tumor bearing mice treated with a death receptor (DR)-5 antibody, conatumumab.

2. Materials and methods

2.1. Kit formulations

Duramycin (>90% purity), SnCl_2 (98% purity), $\text{SnCl}_2 \cdot 2\text{H}_2\text{O}$ (98% purity) and tricine (99% purity) were purchased from Sigma-Aldrich,

USA. TPPTS (95.9% purity) was purchased from Strem Chemicals, Inc., USA. HYNIC-NHS (>90% purity) was obtained from MTTI, Inc., USA. HYNIC-duramycin was prepared as previously described [28]. Three different single-step kits were prepared for ^{99m}Tc -labeling of duramycin. Formulation A consisted of a freeze-dried mixture of 15 μg HYNIC-duramycin, 30 mg tricine, 9.5 mg TPPTS and 6.2 μg SnCl_2 . Formulation B consisted of 5 μg HYNIC-duramycin, 10 mg tricine, 3.2 mg TPPTS and 5.1 μg $\text{SnCl}_2 \cdot 2\text{H}_2\text{O}$. Formulation C consisted of 20 μg HYNIC-PEG₁₂-duramycin, 30 mg tricine, 9.5 mg TPPTS and 15 μg $\text{SnCl}_2 \cdot 2\text{H}_2\text{O}$.

2.2. Radiolabeling and purification of ^{99m}Tc duramycin

Approximately 984.23 ± 190.65 MBq of ^{99m}Tc pertechnetate in 0.5 mL of saline was added to the kits followed by heating at 80 °C for 20 min. The obtained ^{99m}Tc duramycin was either used without purification or purified using reverse phase high-performance liquid-chromatography (RP-HPLC) or using a reversed phase (RP) solid-phase extraction (SPE) method. For RP-HPLC purification, a C₁₈ column (Grace Vydac 218TP, 5 μm , 300 Å, 250 × 4.6 mm) was used with a gradient elution of 10 mM NaH_2PO_4 pH 6.7 and acetonitrile at a flow rate of 1 mL/min and UV/VIS ($\lambda = 215$ nm, SPD-20A UV/VIS detector, Shimadzu, Japan) and radiodetection (NaI scintillation detector, Raytest, Germany). ^{99m}Tc duramycin ($R_t = 16$ min) was collected and solvents were evaporated under a gentle stream of N_2 . The radiotracer was reconstituted in saline with 5% ethanol for *in vivo* use. For SPE purification of kit prepared ^{99m}Tc duramycin, an Oasis HLB (hydrophilic-lipophilic balanced) Plus short cartridge (225 mg, 60 μm , Waters, USA) was conditioned using 3 mL of ethanol 96%, followed by 3 mL of H_2O . The whole reaction mixture was applied to the SPE cartridge followed by a wash step with 3 mL of H_2O and elution of the cartridge with 2 mL of 96% ethanol. The ethanol was evaporated under a gentle stream of N_2 , and the radiotracer was reconstituted in saline with 5% ethanol for *in vivo* use. Radiochemical purity (RCP) was assessed by analytical HPLC using the same method as described above for the purification and by radio-ITLC (NaI scintillation detector, Raytest, Germany), using iTLC silica gel strips (Merck KGaA, Germany) and 20% NaCl and H_2O as mobile phases.

2.3. *In vivo* evaluation of different kit compositions and impact of purification

All experimental procedures and protocols were performed according with European Directive 86/609/EEC Welfare and Treatment of Animals and were approved by the local ethical commission (2014-26, University of Antwerp, Belgium). Animals were bought from Charles River Laboratories (Belgium), and group-housed in individually ventilated, enriched cages with *ad libitum* access to food and water.

Female CD1 $-\text{}/-\text{}$ nude mice weighing 19–23 g were intravenously (i.v.) injected with ~37 MBq of non-purified ^{99m}Tc duramycin (kits A, B, and C; $n = 3$ for each formulation), HPLC-purified (kit A, $n = 3$) or SPE purified ^{99m}Tc duramycin (kit A and B; $n = 3$ for each formulation) via lateral tail vein injection. Twenty-four hours after the injection of the radiotracer, blood was collected through cardiac puncture and the mice were euthanized via cervical dislocation for *ex vivo* biodistribution studies. Organs and tissues were harvested, rinsed in PBS, weighed and the radioactivity was measured in an automated gamma counter (Wizard² 2480, Perkin Elmer, USA) using an energy window of 140 ± 19 keV. Uptake of ^{99m}Tc duramycin is presented as percentage of injected dose per gram (%ID/g).

2.4. Evaluation of species difference

Healthy female Sprague-Dawley rats (6–9 weeks old) weighing 250–270 g were i.v. injected with ~370 MBq of non-purified ^{99m}Tc duramycin (kit A, $n = 3$) via lateral vein injection. Twenty-four hours after tracer injection, rats were euthanized via i.v. injection of Nembutal

(200 mg/kg, Ceva Santé Animal, Belgium) for *ex vivo* biodistribution. Organs and tissues were harvested, rinsed in PBS, blotted dry, weighed and counted for radioactivity using an automated gamma counter as described above.

2.5. SPECT/CT imaging of treatment response to conatumumab

COLO205 semi-adherent human colorectal adenocarcinoma cells (ATCC-CCL-222, Perkin Elmer, Belgium) were grown in RPMI 1640 medium supplemented with 2 mM L-glutamine, 100 U/mL penicillin plus 100 mg/ml streptomycin (Life Technologies, Belgium), 10% fetal bovine serum and 1 mM sodium pyruvate at 37 °C in a humidified atmosphere containing 5% CO₂. The cells were kept in exponential growth phase by routine passage every 2 to 3 days. COLO205 cells (2×10^6) were subcutaneously inoculated in both hind legs of 5–6 weeks old CD1 –/– female nude mice (n = 6), weighing 19–23 g, as previously described [29]. Tumor volume was measured using a digital caliper and monitored before drug administration (baseline) and the day after the therapy. Tumor volumes were calculated according to the formula: (length \times width²)/2.

Two weeks after inoculation, when the tumors reached an approximate volume of 350 mm³, mice were i.v. injected with 31.92 ± 4.21 MBq of non-purified [^{99m}Tc]duramycin (Kit B, n = 3) or 42.33 ± 3.98 MBq of non-purified [^{99m}Tc]PEG₁₂-duramycin (Kit C, n = 3) for baseline SPECT/CT imaging. Four hours after radiotracer injection mice underwent a 30 min SPECT scan (six frames of 5 min) followed by a CT scan to obtain anatomical information for segmentation using a μ SPECT/CT scanner (VECTor/CT, MILabs, The Netherlands) equipped with a rat multipinhole SPECT collimator as previously described [25]. During imaging, mice were kept under isoflurane anesthesia (2% supplemented with oxygen) and body temperature was kept constant using a heating pad.

The following day, conatumumab (Amgen Inc, USA), a fully human monoclonal antibody directed against human death-receptor 5, was administered via intra-peritoneal (i.p.) injection (30 μ g dissolved in 100 μ l of saline), as previously described [30]. Twenty-four hours later, mice underwent a post-treatment SPECT/CT static scan as described above. After the scan, blood was collected through cardiac puncture and the mice were euthanized via cervical dislocation for *ex vivo* biodistribution and immunohistochemical (IHC) analysis of the tumors.

SPECT images were reconstructed with ordered subset expectation maximization (10 iterations, 16 subsets) and 1.2 mm³ voxel size, and smoothed with a three dimensional isotropic Gaussian filter of 1.5 mm for visualization purposes. Volumes of interest (VOIs) were delineated manually for spleen, liver, kidneys and tumors on the acquired CT images, using PMOD v3.3 (PMOD Technologies, Switzerland). Tracer uptake was quantified from the delineated VOIs, as: [total radioactivity concentration in the tissue at the time of scan (kBq/cc)/total radioactivity injected (kBq)] \times 100 (%ID/cc).

2.6. Blocking study

For the blocking experiment, immunodeficient female CD1 –/– nude mice (n = 21) were inoculated with COLO205 (2×10^6) in both hind legs, as described above. Two weeks after inoculation, mice were treated with irinotecan (80 mg/kg, i.p.) in combination with oxaliplatin (5 mg/kg, i.p.) (n = 18) on alternating days or with vehicle (0.9% NaCl or 5% glucose; n = 3) as previously described [24]. Twenty-four hours after the last treatment, cold duramycin (0.01 μ g, 0.1 μ g, 1 μ g or 50 μ g) was injected i.v. (n = 3/concentration) followed by an i.v. injection with [^{99m}Tc]duramycin (~37 MBq; HPLC purified kit A) 30 min later. The two groups of chemotherapy treated animals that did not receive cold duramycin were iv injected with either HPLC purified kit A (n = 3) or non-purified kit A (n = 3). The vehicle treated group received HPLC purified kit A (n = 3). Four hours after radiotracer injection, mice underwent a SPECT/CT static scan as described above. After the

scan, blood was collected through cardiac puncture and the mice were euthanized via cervical dislocation for *ex vivo* biodistribution, autoradiography and IHC analysis of the tumors.

2.7. Autoradiography and immunohistochemical analysis

For autoradiography studies, tumors were embedded and snap-frozen in Tissue-Tek (OCT compound, VWR, USA). Frozen tissue sections (100 μ m) were sliced and exposed to phosphor screen plates (Fujifilm, USA) overnight. Plates were then imaged using a Phosphor Imager system (FLA7000, GE Healthcare, USA).

Adjacent tumor sections (5 μ m) were formalin-fixed and paraffin embedded (FFPE) for IHC analysis (IHC) of apoptosis by immunostaining against cleaved caspase-3 (CC3, Cell Signaling Technology, USA), according to the manufacturer's instructions. For cleaved caspase-3 staining, the appropriate HRP-conjugated secondary antibody (DAKO EnVision, Belgium) was used. Successively, the nuclei of the tissue sections were counterstained using Mayer's hematoxylin (Sigma-Aldrich, USA) and apoptosis was quantified by manually counting CC3-positive cells in three non-sequential whole tumor sections and scored using an upright microscope at $\times 400$ magnification (Olympus CX31, USA).

2.8. Statistical analysis

All data are expressed as mean \pm standard deviation. Statistical analysis between data sets was performed by unpaired Student's t test (two tailed) and corrected for multiple comparisons using the Holm-Sidak correction method. Two-way analysis of variance (ANOVA), followed by Tukey test was used for multiple comparisons between groups (GraphPad Prism v6.05, GraphPad Software, USA). The statistical significance was set at $p < 0.05$.

3. Results

3.1. In vivo evaluation of different kit compositions and impact of purification

Single-step duramycin kits consisting of 3 different formulations were prepared for labeling with ^{99m}Tc (Table 1). Kit A was prepared according to the formulation developed by Zhao et al [28] which represents the current gold standard for pre-clinical use [20–23]. Kit B contained 1/3 of the ingredients present in kit A and SnCl₂·2H₂O instead of SnCl₂ as reducing agent. For kit C, PEGylated HYNIC-duramycin was prepared and SnCl₂·2H₂O was used as reducing agent. Preparation of kit A and B resulted in [^{99m}Tc]duramycin with a good RCP ranging between 94% and 97% (Table 1), while kit C resulted in [^{99m}Tc]duramycin with a lower RCP of 86%. For all the kits, HPLC analysis revealed the presence of [^{99m}Tc]pertechnetate (Rt = 3.30 min), and the presence of TPPTS (Rt = 3.30 min), tricine (Rt = 2.83), and HYNIC-duramycin (Rt = 19.20 min) in the UV chromatogram (Supplemental Fig. 1). HPLC purification of kit A increased the RCP from $94.93 \pm 3.63\%$ to 100% by removing the [^{99m}Tc]pertechnetate. Furthermore, HPLC purification resulted in a significant reduction of TPPTS, tricine, and HYNIC-duramycin (Supplemental Fig. 1D). SPE purification of kit A and B on the other hand could not completely eliminate the presence of [^{99m}Tc]pertechnetate yet greatly reduced the presence of tricine, and to a lesser extent TPPTS (Supplemental Fig. 1).

Fig. 1 shows the effect of formulation and purification method on liver, spleen and kidney uptake in mice at 24 h post tracer injection. HPLC purified (HP) kit A demonstrated the best biodistribution profile with low uptake in the liver (1.66 ± 0.50 vs 14.69 ± 1.89 %ID/g for non-purified (NP) kit A, $p = 0.0001$), as well as in kidneys (6.98 ± 0.73 vs 14.21 ± 7.60 %ID/g for NP kit A, $p = 0.0134$) and spleen (2.04 ± 0.61 vs 4.80 ± 0.80 %ID/g for NP kit A, $p = 0.4194$). Surprisingly, SPE purification of kit A resulted in a significantly increased liver uptake when compared to NP kit A (21.57 ± 3.28 vs 14.69 ± 1.89 %ID/g for

Table 1
Composition, purification methods and radiochemical purity (RCP) of the different [^{99m}Tc]duramycin formulations.

Kit	Composition	Purification ^a	RCP
A	HYNIC-duramycin 15 µg Tricine 30 mg, TPPTS 9.5 mg, SnCl ₂ 6.2 µg	NP	94.93 ± 3.63% (n = 5)
		SP	97.5% (n = 1)
		HP	100% (n = 1)
B	HYNIC-duramycin 5 µg Tricine 10 mg, TPPTS 3.2 mg, SnCl ₂ ·2H ₂ O 5.1 µg	NP	97.10 ± 0.55% (n = 5)
		SP	98.79 ± 1.72% (n = 2)
C	HYNIC-PEG ₁₂ -duramycin 20 µg, Tricine 30 mg, TPPTS 9.5 mg, SnCl ₂ ·2H ₂ O 15 µg	NP	86.00 ± 0.71% (n = 3)

^a Non-purified (NP); SPE purified (SP); HPLC purified (HP)

NP kit A, $p = 0.0183$), while uptake in the kidneys was significantly lower (7.76 ± 0.86 vs 14.21 ± 7.60 %ID/g for NP kit A, $p = 0.0268$). Only minimal impact was visible for the spleen uptake (4.94 ± 1.50 vs 4.80 ± 0.80 %ID/g).

The use of NP kit B which contains one-third of the ingredients and SnCl₂·2H₂O instead of SnCl₂ in comparison to kit A, significantly improved the PK profile with reduced liver (3.60 ± 0.29 %ID/g, $p = 0.0002$ compared to NP kit A), spleen (1.90 ± 0.29 %ID/g, $p = 0.5677$ compared to NP kit A) and kidney uptake (5.49 ± 1.02 %ID/g, $p = 0.0033$ compared to NP kit A). SPE purification of kit B increased the kidney uptake (6.97 ± 0.56 vs. 5.49 ± 1.02 %ID/g for NP kit B) and had only a minor impact on liver and spleen uptake.

PEGylated HYNIC-duramycin (kit C, NP) demonstrated a spleen (1.59 ± 0.57 %ID/g) and kidney uptake (7.50 ± 0.50 %ID/g) comparable to what was observed for HP kit A while liver uptake was slightly higher (4.66 ± 1.37 %ID/g).

3.2. Evaluation of species difference

As previously published data on the use of NP kit A in rats [18] did not report on high non-specific accumulation in liver, spleen and kidneys, we performed a comparative biodistribution study in healthy rats and nude mice at 24 h post tracer injection. In contrast to the biodistribution profile obtained with NP kit A in mice, rats demonstrated a significantly lower uptake in the liver (0.28 ± 0.05 %ID/g; $p = 0.0002$), spleen (1.39 ± 0.64 %ID/g; $p = 0.0045$) and kidneys (1.22 ± 0.21 %ID/g; $p = 0.0416$) (Fig. 2).

3.3. Blocking study

Pre-treatment of chemotherapy treated COLO205 tumor bearing mice with 0.01 µg of cold duramycin prior to injection of [^{99m}Tc]duramycin (HP kit A) did not significantly alter uptake of radioactivity in liver, spleen and kidneys compared to non-blocked HP kit (Fig. 3).

Increasing the amount of cold duramycin to 0.1 µg led to an increased kidney uptake (21.94 ± 7.52 %ID/g, $p = 0.0305$, compared to non-blocked HP kit A) with almost no effect on liver (2.00 ± 0.46 %ID/g) and spleen (0.82 ± 0.15 %ID/g) uptake. Pre-injection of 1 µg duramycin further increased the kidney uptake (35.94 ± 2.6 %ID/g, $p < 0.001$ compared to non-blocked HP kit A) and additionally increased uptake of radioactivity in both spleen (3.25 ± 2.98 %ID/g) and liver (6.51 ± 3.2 %ID/g). As also demonstrated by µSPECT/CT images in Fig. 4, pre-treatment with 50 µg of cold duramycin had the most significant impact on liver (43.1 ± 2.6 , $p < 0.001$ compared to non-blocked HP kit A) and spleen uptake (126.2 ± 10.6 %ID/g, $p < 0.001$ compared to non-blocked HP kit A) with accumulation of radioactivity in those organs even surpassing the uptake demonstrated for NP kit A (31.40 ± 10.62 %ID/g for liver and 18.58 ± 9.54 %ID/g for spleen). Uptake in the kidneys on the other hand decreased (4.59 ± 0.82 %ID/g) and was lower than the kidney uptake for NP kit A (13.18 ± 0.39 %ID/g) and for non-blocked and blocked (0.01–1 µg) HP kit A.

We previously demonstrated that treatment of COLO205 xenografts with a combination of irinotecan and oxaliplatin results in increased apoptotic levels which correlate well with the uptake of [^{99m}Tc]duramycin (HP kit A) in the tumors [24]. In the current study the use of NP kit A resulted in a significantly lower tumor uptake compared to HP kit A (0.89 ± 0.32 %ID/g and 2.10 ± 0.61 %ID/g, respectively (Fig. 5A). Pre-treatment of the mice with cold duramycin significantly decreased tracer uptake (HP kit A) in chemotherapy treated tumors in a dose dependent manner. The reduction in tumor uptake when pre-treating animals with cold duramycin or when using NP kit A was also demonstrated by *ex vivo* autoradiography of excised tumors (Fig. 5B).

3.4. SPECT/CT imaging of treatment response to conatumumab

Since the use of NP kit B, NP kit C and HP kit A resulted in the lowest non-specific accumulation of radioactivity in mice at 24h p.i., the usefulness of the kits for cell death imaging was compared in a treatment

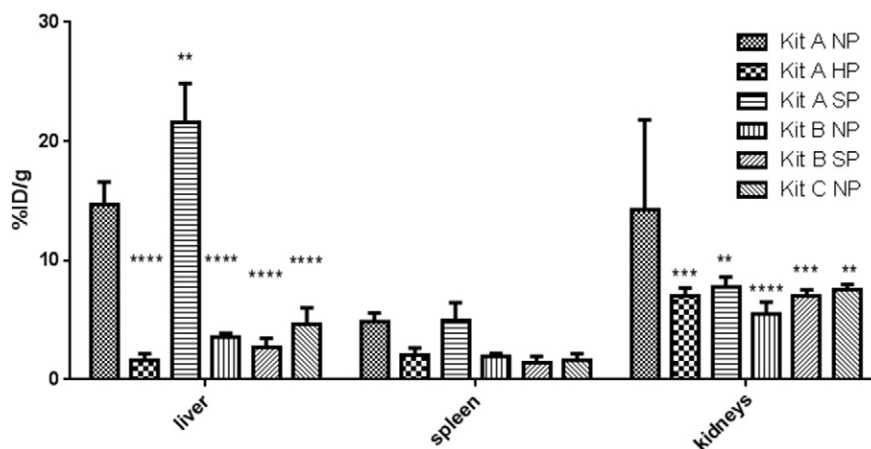


Fig. 1. *Ex vivo* biodistribution in nude mice 24 h p.i. of different [^{99m}Tc]duramycin kit formulations (A, B, C) with different purification methods (NP = non-purified, SP = SPE purified, HP = HPLC purified; n = 3/condition). Data are expressed as percent injected dose per gram of tissue (%ID/g ± SD). Two way ANOVA with Bonferroni multiple comparison correction: **** $p < 0.0001$; *** $0.0001 < p < 0.01$; ** $p < 0.01$ significantly different from kit A NP.

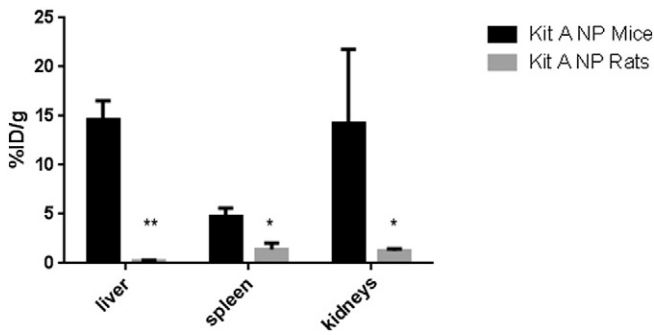


Fig. 2. Ex vivo biodistribution in mice ($n = 3$) and rats ($n = 3$) 24 h p.i. of NP kit A. Data are expressed as percent injected dose per gram tissue (%ID/g \pm SD). Multiple t-tests with Holm–Sidak correction ** $p < 0.001$; * $p < 0.05$.

response evaluation study. More specifically, the cell death targeting capacity with targeted therapy treated COLO205 xenografts of NP kit B and C was compared to previously obtained imaging data using HP kit A at 4 h p.i. [30]. Twenty-four hours post treatment and 4 h post tracer injection, HP kit A demonstrated the highest tumor uptake (5.21 ± 1.71 %ID/cc) and the highest increase compared to baseline (0.64 ± 0.08 %ID/g at baseline, 7 fold increase; $p < 0.001$) (Fig. 6B). Tumor uptake for NP kit B was also low at baseline (0.35 ± 0.07 %ID/g) and significantly increased 3.83 fold after treatment (1.68 ± 0.46 %ID/cc; $p = 0.0078$). Tumor uptake of [^{99m}Tc]PEG₁₂-duramycin (NP Kit C) was equally low at baseline (0.44 ± 0.20 %ID/cc) but did not significantly increase 24 h after treatment (0.84 ± 0.35 %ID/cc).

Ex vivo biodistribution confirmed the higher tumor uptake for NP kit B (2.52 ± 1.10 %ID/g) compared to NP kit C (1.10 ± 0.18 %ID/g; $p = 0.0043$) (Fig. 6C). As was also visible in the SPECT images (Fig. 6A), ex vivo biodistribution of NP kit C at 4 h p.i. showed a high uptake of radioactivity in the liver (16.45 ± 2.78), spleen (7.55 ± 1.51) and kidneys (15.51 ± 3.76), while this high uptake was not visible in the biodistribution study performed at 24 h p.i.

Immunohistochemical analysis of the tumors demonstrated that the level of cleaved caspase-3 (CC3) positive cells in the treated tumors was not significantly different between the groups ($31.2 \pm 10.7\%$, $30.8 \pm 11.4\%$ and $28.9 \pm 6.6\%$, respectively for HP kit A, NP kit B and C; $p = 0.8652$). For all the groups, levels of CC3+ were significantly different from those in tumors of mice treated with an IgG1 isotype control mAb ($1.5 \pm 0.5\%$, $p < 0.0001$).

4. Discussion

In recent years molecular imaging of cell death has gained interest in oncology for monitoring tumor response to cancer therapy. [^{99m}Tc]duramycin is a peptide based radiotracer which has been used in different animal models for *in vivo* visualization of cell death [19–27]. The aim of the present study was to evaluate the impact of purification, kit composition and species difference on the PK profile and cell death targeting properties of [^{99m}Tc]duramycin in order to define the optimal conditions for (pre-)clinical use of kit prepared [^{99m}Tc]duramycin.

We evaluated the use of an Oasis HLB cartridge for the SPE purification of kit prepared [^{99m}Tc]duramycin. The cartridge contains a polymeric hydrophilic–lipophilic balanced sorbent which is suitable for the extraction of both polar and apolar analytes [31]. Washing of the cartridge with water prior to elution of the [^{99m}Tc]duramycin efficiently reduced the amount of [^{99m}Tc]pertechnetate, tricine, and to a lesser extent TPPTS, present in the reaction mixture. Yet the highest purity could still be obtained by applying HPLC purification. This higher purity was also reflected in the biodistribution study of kit A at 24 h post tracer injection showing the lowest kidney and liver accumulation when HPLC purification was applied. This positive effect on kidney uptake was also demonstrated for SPE purified kit A, although it also resulted in a significantly higher accumulation of radioactivity in the liver. The potential effect of co-ligands on the biodistribution profile and excretion kinetics of ^{99m}Tc -labeled radiotracers has been previously reported in the literature [32–38]. Yet, different effects have been described. The use of TPPTS for example resulted in high liver accumulation and low target uptake when used for ^{99m}Tc -labeling of a HYNIC-IL-8 conjugate [34] while when used for ^{99m}Tc -labeling of a cyclic RGDfK tetramer, high tumor/liver and tumor/lung ratios were demonstrated [39]. The effect of the co-ligands is thus largely dependent on the targeting molecule present in the formulation [40]. The effect of the purification method on the liver and kidney uptake of [^{99m}Tc]duramycin can thus most likely not solely be explained by a less efficient removal of TPPTS when applying SPE purification instead of HPLC purification. Analysis of the radiochromatograms of [^{99m}Tc]duramycin revealed the presence of several small peaks eluting in the vicinity of the main peak (Supplemental Fig. 2). These peaks are most likely related to the presence of coordination isomers from HYNIC and the co-ligands [41], which might affect the biodistribution of the radiotracer. While through HPLC purification of [^{99m}Tc]duramycin the presence of these presumed isomers could be greatly reduced, SPE purification did not reduce their presence. Nevertheless, the total peak area of the isomers was always $< 10\%$ and individually they did not account for > 2 area %. The presence of isomeric

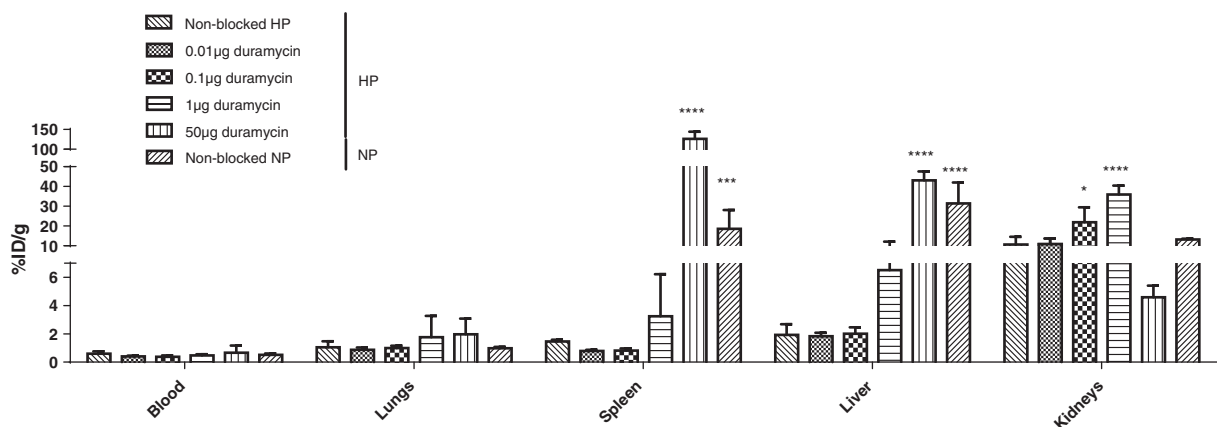


Fig. 3. Ex vivo biodistribution at 4 h post injection of HP or NP kit A in mice pre-treated with different amounts of cold duramycin ($n = 3$ per condition). Data are expressed as percent injected dose per gram of tissue (%ID/g \pm SD). Two-way ANOVA with Bonferroni's method correction for multiple comparison. * $p < 0.05$, *** $p < 0.0005$, **** $p < 0.0001$ significantly different from Non-blocked HP.

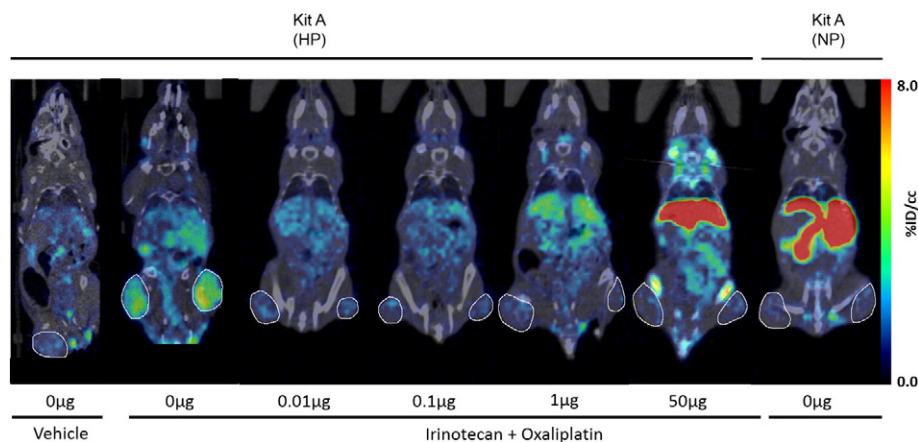


Fig. 4. Representative μ SPECT/CT images at 4 h p.i. of ~ 37 MBq kit A (HP or NP) in chemotherapy or vehicle treated COLO205 tumor bearing CD1 $-/-$ mice pre-injected with different amounts of cold duramycin. Tumors are encircled.

forms is therefore most likely not the only explanation for the different pharmacokinetic behavior witnessed for HPLC purified, SPE purified and non-purified [^{99m}Tc]duramycin. Likewise with HPLC purification, a significant effect on both liver and spleen accumulation of [^{99m}Tc]duramycin could be obtained by lowering the amount of kit ingredients to 1/3 of the amounts present in kit A. The use of kit B resulted in a PK profile almost identical to what could be obtained for HPLC purified kit A. The use of an SPE purification step did not significantly alter the PK profile of kit B, suggesting that this kit can potentially be used without a purification step. These results indicate that the amount of ingredients present in the final formulation indeed is crucial to obtain a favorable PK profile of [^{99m}Tc]duramycin. As NP kit C contains equal amounts of co-ligands compared to NP kit A and did not result in a high liver and kidney uptake, PEGylation of duramycin or the amount of HYNIC-duramycin present in the final formulation might be more important factors than the presence of co-ligands to obtain [^{99m}Tc]duramycin with good imaging characteristics.

Another possible explanation for the liver and spleen uptake of non-purified kit A could be that intermolecular interactions and subsequent formation of duramycin aggregates arise when a threshold concentration of duramycin is exceeded. Aggregates with a size $< 1 \mu\text{m}$ will be phagocytized by the reticuloendothelial system (RES) in the liver and spleen which might explain the accumulation of radioactivity in those organs [42]. By reducing the amount of kit ingredients to 1/3 of the amount present in kit A we presumed that potential aggregate formation could possibly be prevented resulting in a PK profile resembling the one of HPLC purified [^{99m}Tc]duramycin. Although aggregate formation could explain non-specific accumulation of radioactivity in liver and spleen, we were unable to detect aggregates in our HPLC analysis. The Vydac column that was used can separate polypeptides with an MW < 5000 so potentially bigger aggregates are formed which remain trapped in the loop or do not elute from the column. Further research should be dedicated to the development of a different HPLC method which enables the identification of aggregates as well as the formation

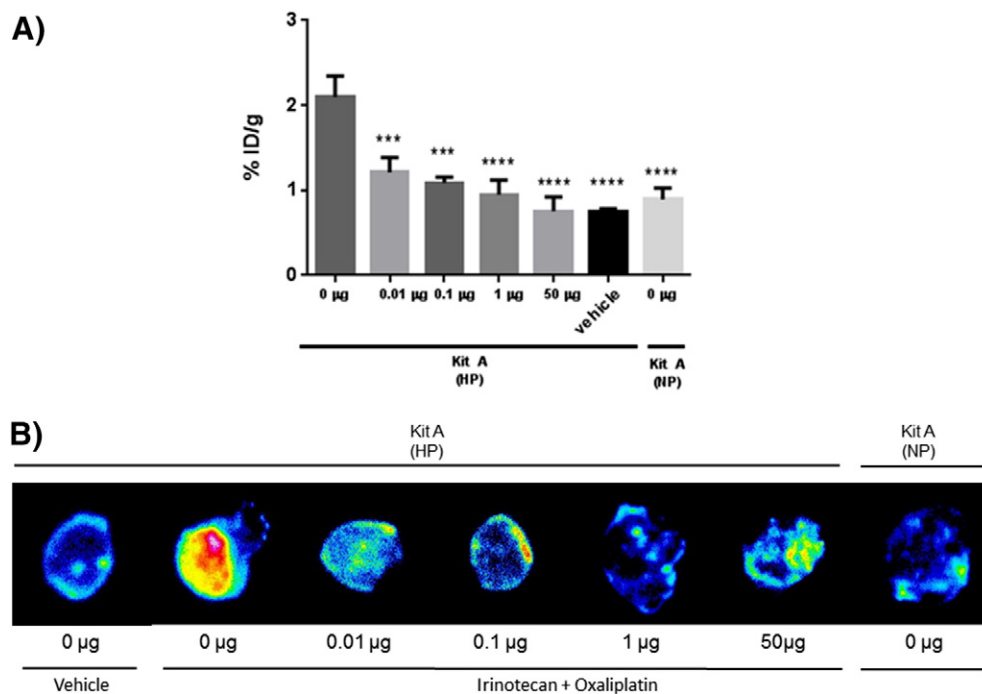


Fig. 5. (A) *Ex vivo* tumor uptake ($\% \text{ID/g} \pm \text{SD}$) at 4 h p.i. of HP or NP kit A in mice pre-treated with different amounts of cold duramycin ($n = 3$ per condition). One-way ANOVA with Holm-Sidak correction. *** $p < 0.001$, **** $p < 0.0001$ compared to non-blocked HP kit A. (B) Representative autoradiography images of COLO205 whole tumor slices from mice treated with combination of irinotecan (80 mg/kg) and oxaliplatin (5 mg/kg) or vehicle (0.9% NaCl/5% glucose on alternate days) at 4 h p.i. injected with HP or NP kit A and pre-treated with different amounts of cold duramycin.

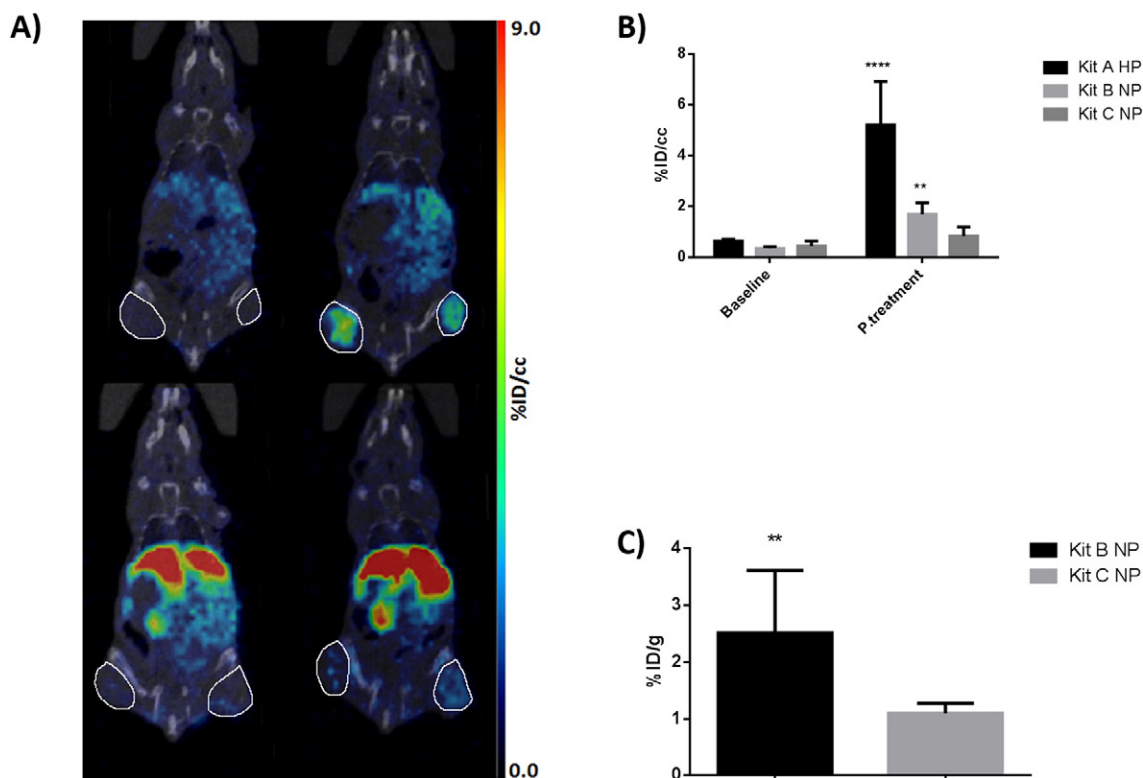


Fig. 6. (A) Representative μ SPECT/CT images of COLO205 tumor bearing CD1 $-/-$ mice 4 h p.i. of ~ 37 MBq NP kit B (upper panels) or NP kit C (lower panels). Baseline (left panels) or post conatumumab treatment (right panels). Tumors are encircled. (B) Quantification of tumor uptake (%ID/cc \pm SD) at baseline and post conatumumab treatment. Two Way ANOVA with Sidak correction. ****: $p < 0.0001$; **: $p < 0.05$ compared to baseline. (C) Ex vivo tumor uptake (%ID/g \pm SD) of [^{99m}Tc]duramycin (NP kit B) or [^{99m}Tc]PEG₁₂-duramycin (NP kit C) at 4 h p.i. Unpaired t-test with Mann-Whitney correction method. **: $p < 0.05$.

of other radiolabeled species not fully resolved by the current HPLC method which might also explain the observed differences in the PK behavior.

Another factor which has been correlated with increased deposition of molecules in liver and spleen is lipophilicity. Attaching polyethylene glycol chains to biomolecules, so called PEGylation, is a technique often used to improve the PK behavior of peptides and proteins. By increasing the overall hydrophilicity of the modified molecule, the elimination pathway can be switched from hepatic to renal [43–45]. The use of kit prepared, non-purified PEGylated [^{99m}Tc]duramycin (kit C) significantly decreased the liver uptake compared to non-purified kit A at 24 h post tracer injection. However, while the effect of PEGylation was clearly visible at 24 h pi, an imaging study at 4 h p.i. demonstrated a different PK profile with high liver, spleen and kidney uptake. PEGylated [^{99m}Tc]duramycin thus requires longer circulation times to obtain a more optimal PK profile excluding tracer injection and imaging within the same day.

As demonstrated before [24] HPLC-purified [^{99m}Tc]duramycin showed excellent cell death targeting properties with high tumor-to-background ratios at 4 h pi. The use of non-purified [^{99m}Tc]duramycin on the other hand resulted in high non-specific uptake of the radiotracer in non-target organs, resulting in insufficient targeting ability and thus low tumor uptake. Pre-treating the animals with cold duramycin in an amount as low as 0.01 μg was able to significantly block the uptake of HPLC-purified [^{99m}Tc]duramycin in treated tumors, again pointing to the importance of using high specific activity [^{99m}Tc]duramycin for cell death imaging. IHC analysis demonstrated chemotherapy induced apoptosis in all the tumors. The dose related reduction in tumor uptake might thus be related to competition of cold duramycin with the radiotracer for binding to PE. Moreover, while pre-treatment of the mice with 0.01 μg and 0.1 μg duramycin had no impact on the PK profile of HPLC-purified [^{99m}Tc]duramycin, pre-treatment of the mice with 1 μg and especially with 50 μg of duramycin greatly increased the uptake of HPLC-

purified [^{99m}Tc]duramycin in liver, spleen and lungs while no effect was visible for the uptake of radioactivity in the blood.

HPLC-purified kit A and non-purified kit B demonstrated the best PK profile and were therefore further investigated in a treatment response study. Both kits showed a significant increase in tumor uptake 24 h post treatment compared to baseline. In spite of their comparable favorable PK profile, the tumor uptake of kit B was significantly lower compared to HPLC-purified [^{99m}Tc]duramycin. While reducing the amount of HYNIC-duramycin in the formulation improves the PK profile, it appears that even lower amounts are required to prevent competition with [^{99m}Tc]duramycin for PE binding as was also demonstrated in the blocking study. We therefore prepared kits containing 1 and 0.1 μg of HYNIC-duramycin, but the obtained radiochemical yields were too low to allow an *in vivo* evaluation (results not shown). Further optimization of these kits is required in order to obtain [^{99m}Tc]duramycin with optimal PK properties and targeting ability. Although cell death induction was comparable in all tumors as demonstrated by IHC analysis, PEGylated [^{99m}Tc]duramycin was not able to pick up the increase in cell death induced by the targeted therapy. This low tumor uptake might be related to a reduced binding affinity, to the high amount of HYNIC-PEG₁₂-duramycin (20 μg) present in the kit which might compete for binding to PE in apoptotic cells or to a reduced availability of radiotracer for tumor targeting due to the high liver, spleen and kidney uptake at the 4 h pi imaging time point.

As non-specific accumulation of [^{99m}Tc]duramycin has not been reported in animal models like rat [46] and porcine [20], we hypothesized that this is a species related phenomenon. A side by side comparison of the PK profile of [^{99m}Tc]duramycin in rats and mice indeed demonstrated a quick clearance of radioactivity from non-target organs, especially liver, spleen and kidneys in rats while this was not the case in mice. Considering the fact that this favorable PK profile has also been demonstrated in pigs which show high genetic similarities with primates [47], we might anticipate that this will also be the case in humans. However, a

first in-human biodistribution study will have to confirm this hypothesis.

5. Conclusions

In this study it was demonstrated that to obtain a favorable biodistribution in mice with low non-specific accumulation and high uptake in targets with increased cell death, [^{99m}Tc]duramycin needs to be prepared with high specific activity. Although reducing the amount of ingredients which are present in the current kit formulation had a positive impact on the PK profile, only an HPLC purification of kit prepared [^{99m}Tc]duramycin was able to combine this favorable PK profile with excellent cell death targeting properties. Nevertheless, this need for HPLC purification appeared to be species related and might possibly not be required for human use. A first in human biodistribution study will have to confirm this hypothesis.

Conflict of interest

Brian Gray and Koon Pak are employees of Molecular Targeting Technologies, Inc.

Acknowledgments

The authors are grateful to Philippe Joye, Caroline Berghmans and Steven Deleye for their technical assistance. Conatumumab (AMG 655) was kindly supplied by Amgen, Inc. This work was funded by Antwerp University and its University Hospital, Antwerp, Belgium, through a departmental position for C.V.; an assistant professor position for L.w.; an associate professor position for S. Staelens and a full professor position for S. Stroobants. F.E. is supported by the University of Antwerp through a geconcentreerde onderzoeksactie (GOA.0135.13). This study was funded by the Research Foundation-Flanders (FWO) via a Research Grant (FWO G038914N).

Appendix A. Supplementary data

Supplementary data to this article can be found online at <https://doi.org/10.1016/j.nucmedbio.2017.08.005>.

References

- [1] Therasse P, Arbuik SG, Eisenhauer EA, Wanders J, Kaplan RS, Rubinstein L, et al. New guidelines to evaluate the response to treatment in solid tumors. European Organization for Research and Treatment of Cancer, National Cancer Institute of the United States, National Cancer Institute of Canada. *J Natl Cancer Inst* 2000;92:205–16.
- [2] Norbury CJ, Zhivotovsky B. DNA damage-induced apoptosis. *Oncogene* 2004;23:2797–808.
- [3] Ricci MS, Zong WX. Chemotherapeutic approaches for targeting cell death pathways. *Oncologist* 2006;11:342–57.
- [4] Meyn RE. Apoptosis and response to radiation: implications for radiation therapy. *Oncology (Williston Park)* 1997;11:349–56 [discussion 56, 61, 65].
- [5] Belhocine TZ, Prato FS. Transbilayer phospholipids molecular imaging. *EJNMMI Res* 2011;1:17.
- [6] Vangestel C, Van de Wiele C, Mees G, Mertens K, Staelens S, Reutelingsperger C, et al. Single-photon emission computed tomographic imaging of the early time course of therapy-induced cell death using technetium 99m tricarbonyl His-annexin A5 in a colorectal cancer xenograft model. *Mol Imaging* 2012;11:135–47.
- [7] Wyffels L, Gray BD, Barber C, Woolfenden JM, Pak KY, Liu Z. Synthesis and preliminary evaluation of radiolabeled bis(zinc(II)-dipicolylamine) coordination complexes as cell death imaging agents. *Bioorg Med Chem* 2011;19:3425–33.
- [8] Wang F, Fang W, Ji SD, Meng QL, Li Y, Fan KW, et al. Technetium-99m labeled synaptotagmin I C2A detection of paclitaxel-induced apoptosis in non-small cell lung cancer. *Zhonghua Zhong Liu Za Zhi* 2007;29:351–4.
- [9] Challapalli A, Kenny LM, Hallett WA, Kozlowski K, Tomasi G, Gudi M, et al. 18F-ICMT-11, a caspase-3-specific PET tracer for apoptosis: biodistribution and radiation dosimetry. *J Nucl Med* 2013;54:1551–6.
- [10] Witney TH, Hoehne A, Reeves RE, Ilovich O, Namavari M, Shen B, et al. A systematic comparison of 18F-C-SNAT to established radiotracer imaging agents for the detection of tumor response to treatment. *Clin Cancer Res* 2015;21:3896–905.
- [11] Su H, Chen G, Gangadharmath U, Gomez LF, Liang Q, Mu F, et al. Evaluation of [18F]-CP18 as a PET imaging tracer for apoptosis. *Mol Imaging Biol* 2013;15:739–47.
- [12] Hoglund J, Shirvan A, Antoni G, Gustavsson SA, Langstrom B, Ringheim A, et al. 18F-ML-10, a PET tracer for apoptosis: first human study. *J Nucl Med* 2011;52:720–5.
- [13] Current Clinical Trials on Annexin V-128 (ClinicalTrials.gov Identifier: NCT02459613; NCT02978885; NCT03232580; NCT02978144; NCT02667457; NCT02182609; NCT02677714).
- [14] Marconescu A, Thorpe PE. Coincident exposure of phosphatidylethanolamine and anionic phospholipids on the surface of irradiated cells. *Biochim Biophys Acta* 1778;2008:2217–24.
- [15] Hayashi F, Nagashima K, Terui Y, Kawamura Y, Matsumoto K, Itazaki H. The structure of PA48009: the revised structure of duramycin. *J Antibiot (Tokyo)* 1990;43:1421–30.
- [16] Zimmermann N, Freund S, Fredenhagen A, Jung G. Solution structures of the lantibiotics duramycin B and C. *Eur J Biochem* 1993;216:419–28.
- [17] Zhao M. Lantibiotics as probes for phosphatidylethanolamine. *Amino Acids* 2011;41:1071–9.
- [18] Zhao M, Li Z, Bugenhagen S. 99mTc-labeled duramycin as a novel phosphatidylethanolamine-binding molecular probe. *J Nucl Med* 2008;49:1345–52.
- [19] Larson MC, Woodliff JE, Hillery CA, Kearn TJ, Zhao M. Phosphatidylethanolamine is externalized at the surface of microparticles. *Biochim Biophys Acta* 2012;1821:1501–7.
- [20] Wang L, Wang F, Fang W, Johnson SE, Audi S, Zimmer M, et al. The feasibility of imaging myocardial ischemic/reperfusion injury using (99m)Tc-labeled duramycin in a porcine model. *Nucl Med Biol* 2015;42:198–204.
- [21] Zhang Y, Stevenson GD, Barber C, Furenlied LR, Barrett HH, Woolfenden JM, et al. Imaging of rat cerebral ischemia-reperfusion injury using (99m)Tc-labeled duramycin. *Nucl Med Biol* 2013;40:80–8.
- [22] Johnson SE, Li Z, Liu Y, Moulder JE, Zhao M. Whole-body imaging of high-dose ionizing irradiation-induced tissue injuries using 99mTc-duramycin. *J Nucl Med* 2013;54:1397–403.
- [23] Audi SH, Jacobs ER, Zhao M, Roerig DL, Haworth ST, Clough AV. In vivo detection of hyperoxia-induced pulmonary endothelial cell death using (99m)Tc-duramycin. *Nucl Med Biol* 2015;42:46–52.
- [24] Elvas F, Vangestel C, Pak KY, Vermeulen P, Gray B, Stroobants S, et al. Early prediction of tumor response to treatment: pre-clinical validation of 99mTc-duramycin. *J Nucl Med* 2016;57:805–11.
- [25] Elvas F, Vangestel C, Rapic S, Verhaeghe J, Gray B, Pak K, et al. Characterization of [(99m)Tc]duramycin as a SPECT imaging agent for early assessment of tumor apoptosis. *Mol Imaging Biol* 2015;17:838–47.
- [26] Luo R, Niu L, Qiu F, Fang W, Fu T, Zhao M, et al. Monitoring apoptosis of breast cancer xenograft after paclitaxel treatment With 99mTc-labeled duramycin SPECT/CT. *Mol Imaging* 2016;15, 1536012115624918.
- [27] Liu Z, Larsen BT, Lerman LO, Gray BD, Barber C, Hedayat AF, et al. Detection of atherosclerotic plaques in ApoE-deficient mice using 99mTc-duramycin. *Nucl Med Biol* 2016;43:496–505.
- [28] Zhao M, Li Z. A single-step kit formulation for the (99m)Tc-labeling of HYNIC-duramycin. *Nucl Med Biol* 2012;39:1006–11.
- [29] Vangestel C, Van de Wiele C, Van Damme N, Staelens S, Pauwels P, Reutelingsperger CP, et al. (99m)Tc-(CO)(3) His-annexin A5 micro-SPECT demonstrates increased cell death by irinotecan during the vascular normalization window caused by bevacizumab. *J Nucl Med* 2011;52:1786–94.
- [30] Elvas F, Boddaert J, Vangestel C, Pak K, Gray B, Kumar-Singh S, et al. 99mTc-duramycin SPECT imaging of early tumor response to targeted therapy: a comparison with 18F-FDG PET. *J Nucl Med* 2017;58:665–70.
- [31] Chitneni SK, Serdons K, Evens N, Fonge H, Celen S, Deroose CM, et al. Efficient purification and metabolite analysis of radiotracers using high-performance liquid chromatography and on-line solid-phase extraction. *J Chromatogr A* 2008;1189:323–31.
- [32] Decristoforo C, Mather SJ. Technetium-99m somatostatin analogues: effect of labelling methods and peptide sequence. *Eur J Nucl Med* 1999;26:869–76.
- [33] Decristoforo C, Mather SJ. 99m-Technetium-labelled peptide-HYNIC conjugates: effects of lipophilicity and stability on biodistribution. *Nucl Med Biol* 1999;26:389–96.
- [34] Rennen HJ, van Eerd JE, Oyen WJ, Corstens FH, Edwards DS, Boerman OC. Effects of coligand variation on the in vivo characteristics of Tc-99m-labeled interleukin-8 in detection of infection. *Bioconjug Chem* 2002;13:370–7.
- [35] Babich JW, Fischman AJ. Effect of "co-ligand" on the biodistribution of 99mTc-labeled hydrazino nicotinic acid derivatized chemotactic peptides. *Nucl Med Biol* 1995;22:25–30.
- [36] Babich JW, Graham Coco W, Barrow S, Fischman AJ, Femia FJ, Zubieta J. 99mTc-labeled chemotactic peptides: influence of coligand on distribution of molecular species and infection imaging properties. Synthesis and structural characterization of model complexes with the {Re(η²-HN(C5H4N)(η¹-NN(C5H4N))} core. *Inorg Chim Acta* 2000;309:123–36.
- [37] Barrett JA, Crocker AC, Dampousse DJ, Heminway SJ, Liu S, Edwards DS, et al. Biological evaluation of thrombus imaging agents utilizing water soluble phosphines and tricine as coligands when used to label a hydrazinonicotinamide-modified cyclic glycoprotein IIb/IIIa receptor antagonist with 99mTc. *Bioconjug Chem* 1997;8:155–60.
- [38] Liu S, Hsieh WY, Kim YS, Mohammed SI. Effect of coligands on biodistribution characteristics of ternary ligand 99mTc complexes of a HYNIC-conjugated cyclic RGDfK dimer. *Bioconjug Chem* 2005;16:1580–8.
- [39] Liu S, Hsieh WY, Jiang Y, Kim YS, Sreerama SG, Chen X, et al. Evaluation of a (99m)Tc-labeled cyclic RGD tetramer for noninvasive imaging integrin α_vβ₃-positive breast cancer. *Bioconjug Chem* 2007;18:438–46.
- [40] Liu S, Kim YS, Hsieh WY, Gupta Sreerama S. Coligand effects on the solution stability, biodistribution and metabolism of the (99m)Tc-labeled cyclic RGDfK tetramer. *Nucl Med Biol* 2008;35:111–21.
- [41] Edwards DS, Liu S, Barrett JA, Harris AR, Looby RJ, Ziegler MC, et al. New and versatile ternary ligand system for technetium radiopharmaceuticals: water soluble

- phosphines and tricine as coligands in labeling a hydrazinonicotinamide-modified cyclic glycoprotein IIb/IIIa receptor antagonist with ^{99m}Tc . *Bioconjug Chem* 1997;8:146–54.
- [42] Saklad EL. Albumin microaggregates for radioactive scanning of reticuloendothelial systems. Google Patents; 1980.
- [43] Webster R, Didier E, Harris P, Siegel N, Stadler J, Tilbury L, et al. PEGylated proteins: evaluation of their safety in the absence of definitive metabolism studies. *Drug Metab Dispos* 2007;35:9–16.
- [44] Hoppmann S, Hirani E, McRobbie G, Hiscock D. Detection of cell death with GE152 in a small animal model: a tool for early assessment of tumour therapy response. WMIC conferenceConference paper; 2012.
- [45] Varasteh Z, Rosenstrom U, Velikyan I, Mitran B, Altai M, Honarvar H, et al. The effect of mini-PEG-based spacer length on binding and pharmacokinetic properties of a ^{68}Ga -labeled NOTA-conjugated antagonistic analog of bombesin. *Molecules* 2014;19:10455–72.
- [46] Audi S, Li Z, Capacete J, Liu Y, Fang W, Shu LG, et al. Understanding the in vivo uptake kinetics of a phosphatidylethanolamine-binding agent (^{99m}Tc)-Duramycin. *Nucl Med Biol* 2012;39:821–5.
- [47] Yu H, Wu Q, Zhang J, Zhang Y, Lu C, Cheng Y, et al. Genome-wide characterization of PRE-1 reveals a hidden evolutionary relationship between suidae and primates. *BioRxiv* 2015. <https://doi.org/10.1101/025791>.